Inorganic Chemistry

Article

pubs.acs.org/IC

Lanthanide Complexes of Tritopic Bis(hydrazone) Ligands: Single-Molecule Magnet Behavior in a Linear Dy^{III}_3 Complex

Muhammad U. Anwar,[†] Santokh S. Tandon,[‡] Louise N. Dawe,[†] Fatemah Habib,[§] Muralee Murugesu,[§] and Laurence K. Thompson*[,†]

[†]Department of Chemistry, Memorial University, St. John's, Newfoundland A1B 3X7, Canada

[‡]Department of Chemistry, Kent State University at Salem, Salem, Ohio 44460, United States

[§]Department of Chemistry, University of Ottawa, 10 Marie Curie, Ottawa, Ontario K1N 6N5, Canada

Supporting Information

ABSTRACT: Tritopic pyridinebis(hydrazone)-based ligands typically produce square M_9 [3 × 3] grid complexes with first-row transition-metal ions (e.g., M = Mn, Fe, Co, Cu, Zn), but with larger lanthanide ions, such coordination motifs are not produced, and instead linear trinuclear complexes appear to be a preferred option. The reaction of 2pomp [derived from pyridine-2,6-bis(hydrazone) and 2-acetylpyridine] with La^{III}, Gd^{III}, and Dy^{III} salts produces helical linear trinuclear $[Ln_3(2pomp)_2]$-based complexes, where each metal ion occupies one of the three tridentate ligand pockets. Two ligands encompass the three metal ions, and internal connections between metal ions occur through μ-$O_{hydrazone}$ bridges. Coligands include benzoate, nitrate, and *N*,*N*-dimethylformamide. The linear Dy^{III}_3 complex exhibits single-molecule magnet behavior, demonstrated through alternating-current susceptibility measurements. Slow thermal magnetic relaxation was detected in an external field of 1800 Oe, where quantum-tunneling effects were suppressed (U_{eff} = 14 K).

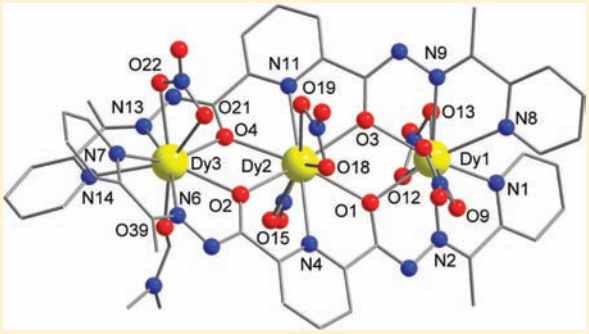

INTRODUCTION

The aggregation of transition-metal ions into polymetallic clusters can be achieved through a programmed approach with polytopic ligands designed to incorporate the metal ions in specific ligand pockets but, at the same time, leaving enough coordination unsaturation that self-assembly leads to clusters and grids. Polytopic hydrazones, e.g., poap, 2poap, and their derivatives (Chart 1; ligands shown as coordinated anions in their *enolic* tautomeric form through proton loss), have proven very effective in producing large numbers of [2 × 2] and [3 × 3] grids with first-row transition-metal ions.[1−9] The principle ligand component responsible for bridging the metal ions in close proximity is the deprotonated hydrazone O atom, which also leads to spin communication between the transition-metal ions.[1−11] The five-membered chelate rings generated with these ligands upon coordination are a good fit for the average first-row transition-metal ion, creating [*n* × *n*] grid cores that are roughly planar, with minor puckering along each metal chain direction. However, when metal ions with larger radii, e.g., Pb^{II}, coordinate, they protrude from each ligand pocket and prevent grid formation. In the case of the complex $[Pb_3(2poap\text{-}2H)(ClO_4)_4]_2{\cdot}8H_2O$, a linear trinuclear structure is obtained, with each metal occupying a tridentate ligand pocket. Longer-range perchlorate bridges link the halves together to form a Pb_6 aggregate structure.[8] Typically, Ln^{III} ions are smaller (102−86.1 pm for Ce^{III} to Lu^{III}) than Pb^{II} (133 pm), and so the possibility of lanthanide [*n* × *n*] grid formation with typical ditopic and tritopic hydrazone ligands encouraged us to explore their lanthanide coordination chemistry. The close proximity of the metal ions in such structures was considered an important feature for the creation of polymetallic systems with potential single-molecule magnet (SMM) behavior.

Chart 1

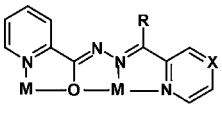

poap-H; (R=NH_2,X=CH),
poapz-H; (R=NH_2,X=N)
pomp-H; (R=CH_3,X=CH)

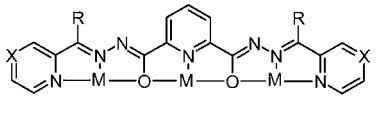

2poap-2H (R=NH_2,X=CH)
2pomp-2H (R=CH_3,X=CH)
2poapz-2H (R=NH_2,X=N)

Received: October 11, 2011
Published: December 22, 2011

   dx.doi.org/10.1021/ic2022006 | *Inorg. Chem.* 2012, 51, 1028−1034

Table 1. Crystallographic Details for Complexes 1−4

	1	2	3	4
chemical formula	$C_{25}H_{33}GdN_{14}O_{15}$	$C_{63.75}H_{73.5}Cl_{1.5}La_3N_{14}O_{27.75}$	$C_{52.5}H_{58.5}Gd_3N_{22.5}O_{22.5}$	$C_{52.5}H_{58.5}Dy_3N_{22.5}O_{22.5}$
MW	926.87	1949.76	1836.43	1852.18
T (K)	153(2)	153(2)	153(2)	153(2)
cryst syst	triclinic	triclinic	triclinic	triclinic
space group	$P\bar{1}$ (No. 2)	$P\bar{1}$ (No. 2)	$P\bar{1}$ (No. 2)	$P\bar{1}$ (No. 2)
a (Å)	10.815(11)	14.846(10)	11.905(5)	18.872(3)
b (Å)	13.614(10)	15.454(11)	15.845(7)	19.993(3)
c (Å)	13.734(6)	20.0135(6)	20.159(9)	20.904(2)
α (deg)	62.54(4)	82.70(13)	73.396(12)	70.781(4)
β (deg)	75.76(8)	70.19(9)	77.423(14)	73.229(6)
γ (deg)	88.08(8)	88.42(15)	83.680(16)	83.396(6)
V (Å^3)	1732(3)	4284(4)	3552(3)	7129.1(17)
Z	2	2	2	4
D_{calc} (g/cm^3)	1.778	1.511	1.717	1.726
μ(Mo Kα) (cm^{-1})	20.11	15.89	28.63	32.04
reflns total	15 963	34 765	27 827	29 228
reflns unique [$I > 2.00\sigma(I)$]	6357	15 978	12 930	26 147
R_{int}	0.0775	0.0243	0.0289	0.0371
R1 [$I > 2.00\sigma(I)$]	0.1275	0.0596	0.0692	0.0316
wR2 (all data)	0.3437	0.1725	0.1852	0.0836

In the present study, the coordination chemistry of the tritopic hydrazone ligands 2poap and 2pomp (Chart 1) has been investigated with some Ln ions. Mononuclear and trinuclear complexes were obtained and were characterized structurally and magnetically. The larger size of the Ln ions compared with transition-metal ions appears to be the major property that prevents the formation of the putative grids, but the organizing elements of the tritopic ligands still bind three metal ions per ligand, as expected. In the case of the linear trinuclear Dy^{III}_3 complex, slow magnetic relaxation and SMM behavior have been demonstrated.

EXPERIMENTAL SECTION

Synthesis of Ligands and Complexes. 2poap[3] and 2pomp[4] were synthesized using published procedures.

*[(2poap)Gd(NO$_3$)$_2$(DMF)$_2$](NO$_3$) (**1**).* A mixture of $Gd(NO_3)_3{\cdot}6H_2O$ (0.10 g, 0.22 mmol) and 2poap (0.050 g, 0.12 mmol) was gently heated in 20 mL of methanol (MeOH) for 20 min. A yellow precipitate formed and was filtered off and dried. The precipitate was dissolved in *N*,*N*-dimethylformamide (DMF) and MeOH (2 mL each), and the solution was then layered with ether. Yellow crystals appeared after 1 day. Yield: 0.022 g, 20%. Elem anal. Calcd for $(C_{19}H_{17}N_9O_2)Gd(NO_3)_3(C_3H_7NO)(H_2O)_{2.5}$: C, 30.52; H, 3.35; N, 21.04. Found: C, 30.58; H, 3.14; N, 20.82. The structure indicates the presence of two coordinated DMF molecules, but the dried bulk sample appears to have been desolvated.

*[(2pomp-2H)$_2$La$_3$(Bz-H)$_3$(H$_2$O)$_5$](ClO$_4$)$_2$(H$_2$O)$_4$ (**2**).* A solution of $La(ClO_4)_3{\cdot}6H_2O$ (0.14 g, 0.25 mmol) in 10 mL of MeOH was added to a suspension of 2pomp (0.050 g, 0.12 mmol) in 20 mL of MeOH with stirring. A 10 mL solution of sodium benzoate (0.050 g, 0.34 mmol) in MeOH was then added to the reaction mixture, which was then refluxed for 6 h. The resulting solution was filtered, and the filtrate was left undisturbed for crystallization. Yellow crystals appeared after 2 weeks. Yield: 0.080 g, 33%. Elem anal. Calcd for $(C_{21}H_{19}N_7O_2)_2La_3(C_7H_5O_2)_3(H_2O)_9(ClO_4)_2$: C, 38.92; H, 3.65; N, 10.09. Found: C, 39.74; H, 3.09; N, 10.37.

*[(2pomp-2H)$_2$Gd$_3$(NO$_3$)$_5$(DMF)](DMF)$_2$ (**3**).* A solution of $Gd(NO_3)_3{\cdot}6H_2O$ (0.10 g, 0.22 mmol) in 10 mL of MeOH was added to a suspension of 2pomp (0.050 g, 0.12 mmol) in 20 mL of MeOH with stirring. The reaction mixture was refluxed for 8.5 h. A pale-yellow solid formed and was separated, washed with MeOH, and dried. The precipitate was then dissolved in DMF and MeOH (2 mL each), and the solution was layered with ethyl ether. Yellow crystals appeared after 1 day. Yield: 0.080 g, 36%. Elem anal. Calcd for $(C_{21}H_{17}N_7O_2)_2Gd_3(NO_3)_5(C_3H_7NO)_3(H_2O)_{3.5}$: C, 32.99; H, 3.32; N, 16.52. Found: C, 32.79; H, 2.90; N, 16.22.

*[(2pomp-2H)$_2$Dy$_3$(NO$_3$)$_5$(DMF)](DMF) (**4**).* A mixture of $Dy(NO_3)_3{\cdot}6H_2O$ (0.10 g, 0.28 mmol) and 2pomp (0.050 g, 0.12 mmol) was gently heated in 20 mL of MeOH for 40 min and then stirred at room temperature for 1 h. A yellow precipitate formed and was separated by filtration, dried, and then dissolved in DMF. The solution was then layered with ether. Yellow crystals appeared after 1 day. Yield: 0.047 g, 20%. Elem anal. Calcd for $(C_{21}H_{17}N_7O_2)_2Dy_3(NO_3)_5(C_3H_7NO)_3(H_2O)_4$: C, 32.36; H, 3.33; N, 16.29. Found: C, 32.53; H, 2.92; N, 16.03.

X-ray Crystallography. *Experimental Details.* Crystals of **1**−**4** were mounted on low-temperature diffraction loops and measured on a Rigaku Saturn CCD area detector with graphite-monochromated Mo Kα radiation. Structures were solved by direct methods[12] and expanded using Fourier techniques.[13] Neutral atom scattering factors were taken from Cromer and Waber.[14] Anomalous dispersion effects were included in Fcalc.[15] The values for $\Delta f'$ and $\Delta f''$ were those of Creagh and McAuley.[16] The values for the mass attenuation coefficients are those of Creagh and Hubbell.[17] All calculations were performed using *CrystalStructure*[18,19] and *PLATON*[20] crystallographic software packages, except for refinement, which was performed using *SHELXL-97*.[12] Non-H atoms were refined anisotropically, while H atoms were introduced in calculated positions and refined on a riding model, unless otherwise indicated.

For **1** and **3** collection, solution and refinement proceeded normally. For **1**, two lattice solvent water (H_2O) molecules were present in the asymmetric unit. The corresponding H atoms could not be located in difference map positions and were, therefore, omitted from the model; they were included in the formula for calculation of the intensive properties. For **3**, the occupancy of the DMF molecules that contained O21−O23 was refined and converged to 2.3 lattice solvent DMF molecules. The formula has been adjusted to reflect this noninteger value. Similarity restraints were applied to the DMF molecules containing O21 and O23.

For **2** and **4**, the *PLATON*[20] *SQUEEZE* procedure was applied. For **2**, 188 electrons per unit cell were recovered in one void that was sufficiently large to contain a small molecule (total volume 1102 Å^3), that is, 94 electrons per formula unit. Disordered, partial occupancy perchlorate was detected prior to the application of *SQUEEZE*; however, only the Cl position could be identified, and anisotropic refinement was not possible. Further, disordered, partial occupancy

dx.doi.org/10.1021/ic2022006 | *Inorg. Chem.* 2012, 51, 1028−1034

Table 2. Summary of Important Bond Distances (Å) and Angles (deg) for 1− 4

compound	M−O (Å)	M−N (Å)	M−O−M (deg)
1	2.342(11)−2.489(13)	2.577(13)	
2	2.451(3)−2.643(5)	2.631(4)−2.778(6)	109.69(14)−117.90(14)
3	2.303(5)−2.535(7)	2.503(6)−2.635(6)	116.18(19)−117.57(19)
4	2.292(2)−2.535(3)	2.471(3)−2.629(3)	116.55(9)−117.78(9)

latticed solvent H_2O molecules were also detected. This accounts for 50 electrons for ClO_4^- and 40 electrons from four H_2O molecules. H_2O molecules that were directly coordinated to the metal sites were not treated via *SQUEEZE*. Those H atoms were introduced in calculated positions and were refined positionally with isotropic displacements 1.5 times that of the corresponding O atom; distance and angle restraints were applied in their refinement. Similarity restraints were applied to the benzene ring consisting of C58−C63.

For **4**, 216 electrons per unit cell were recovered by *SQUEEZE*,[20] in one void (total volume 1228 Å^3), that is, 54 electrons per formula unit. Lattice solvent DMF molecules (40 electrons/DMF) were present, and the electrons recovered by *SQUEEZE* were assigned as one additional DMF. *PLATON*'s[20] *ADDSYM* detected a pseudotranslation; however, *PLATON*'s SPGRfromEX confirmed the assigned space group.

For both **2** and **4**, molecules omitted from the model by *SQUEEZE* were included in the formula for calculation of the intensive properties. The application of *SQUEEZE* gave a good improvement in the data statistics and allowed for a full anisotropic refinement of both structure models.

RESULTS AND DISCUSSION

Structural Details. *[(2poap)Gd(NO$_3$)$_2$(DMF)$_2$](NO$_3$) (**1**).* Crystallographic details for **1** are listed in Table 1, and a summary of important bond distances and angles is listed in Table 2 (for the full listing, see Table S1 in the Supporting Information). The molecular structure of the cation in **1** is illustrated in Figure 1 (H atoms omitted for clarity). The structure is mononuclear, with a 9-coordinate Gd^{III} ion bound

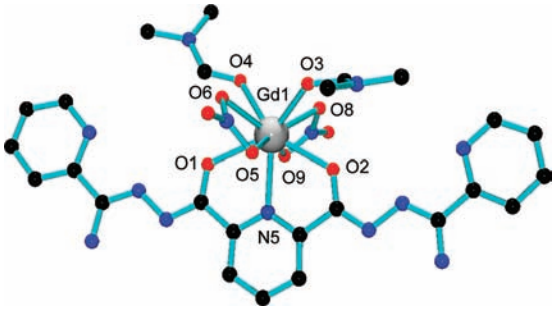

Figure 1. Structural representation for complex **1**.

just in the central NO_2 tridentate pocket of the ligand 2poap. Two bidentate nitrates and two DMF molecules complete the metal coordination sphere. The stoichiometry of the complex based on anion charge indicates that the ligand is neutral, and this is in agreement with ligand bond distances, in particular the hydrazone C−O distances to O1 and O2 [1.239(18) and 1.265(19) Å, respectively], indicating mostly ketonic C═O character. Interestingly, despite the fact that the ligand end pockets are not coordinated, the ligand itself remains remarkably flat, indicating that extended delocalization helps to pin the ligand in this conformation, without the perhaps anticipated rotation of the ends.

*[(2pomp-2H)$_2$La$_3$(Bz-H)$_3$(H$_2$O)$_5$](ClO$_4$)$_2$(H$_2$O)$_4$ (**2**).* Crystallographic details for **2** are listed in Table 1, and a summary of important bond distances and angles is listed in Table 2 (for the full listing see Table S2 in the Supporting Information). The molecular structure of the trinuclear cation in **2** is illustrated in Figure 2 (H atoms omitted for clarity). In contrast to **1**, the

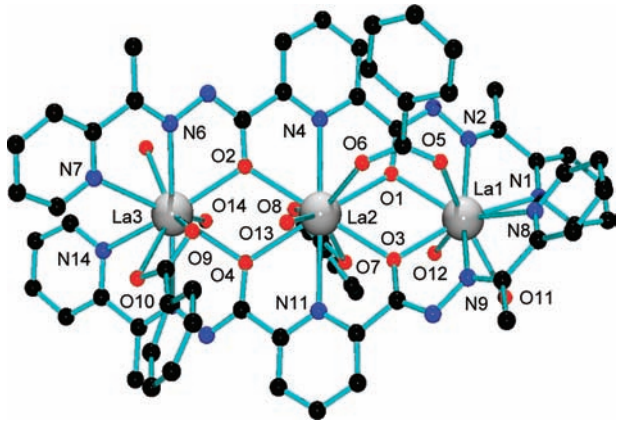

Figure 2. Structural representation for complex **2**.

structure of **2** is trinuclear, with one La^{III} ion occupying each tridentate ligand pocket in the normal way. Two ligands coordinate to the three La^{III} ions in a μ-O-bridging arrangement, with tridentate coordination in each pocket. Three benzoate ions act as coligands, two in chelating bidentate mode to La2 and La3 and one in a 1,3-bridging mode connecting La1 and La2. Four hydrazone μ-O atoms bridge La1, La2, and La3 in sequential pairs, and terminal H_2O molecules occupy the remaining coordination sites. La1 is 9-coordinate, while La2 and La3 are 10-coordinate. The overall structure differs from the trinuclear Pb^{II} derivative[8] (vide supra), which has the three Pb^{II} ions bound to just one ligand. La−ligand distances fall in the range 2.451(3)−2.778(6) Å. La−O−La bridge angles differ considerably, falling in the range 109.69(14)−117.90(14)°, largely as a result of the asymmetric carboxylate bonding arrangement and the presence of just one bridging carboxylate connecting La1 and La2. This is also reflected in the La−La distances [La1−La2 4.225(3) Å; La2−La3 4.370(3) Å].

*[(2pomp-2H)$_2$Gd$_3$(NO$_3$)$_5$(DMF)](DMF)$_2$ (**3**).* Crystallographic details for **3** are listed in Table 1, and a summary of important bond distances and angles is listed in Table 2 (for the full listing, see Table S3 in the Supporting Information). The molecular structure of **3** is illustrated in Figure 3 (H atoms omitted for clarity). The linear trinuclear structure resembles **2**, with a bis-μ-O$_{hydrazone}$ bridge linking adjacent pairs of Gd^{III} ions. Five bidentate chelating nitrate ligands are bound, with one coordinated to Gd1 and two each to Gd2 and Gd3. A DMF molecule is bound to Gd1. Each of the two ligands coordinates in the normal tritopic fashion with each pocket binding in tridentate mode. This leads to a 9-coordinate coordination sphere at Gd1 and a 10-coordinate sphere at Gd2 and Gd3.

dx.doi.org/10.1021/ic2022006 | Inorg. Chem. 2012, 51, 1028−1034

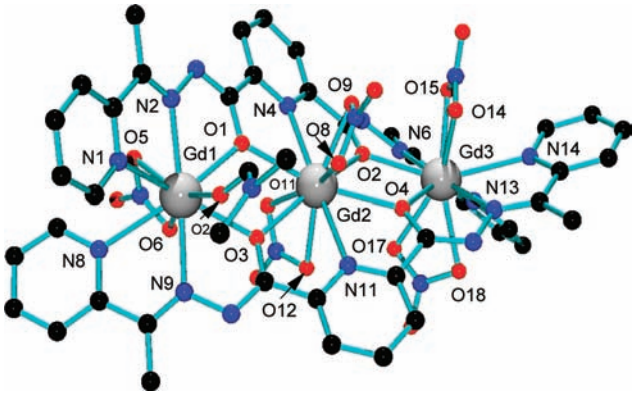

Figure 3. Structural representation for complex **3**.

Gd–ligand distances fall in the range 2.303(5)–2.635(6) Å, and Gd–O–Gd bridge angles fall in the range 116.18(19)–117.57(19)°. Gd1–Gd2 and Gd2–Gd3 distances are 4.125(5) and 4.126(5) Å, respectively.

[(2pomp-2H)$_2$Dy$_3$(NO$_3$)$_5$(DMF)](DMF) (**4**). Crystallographic details for **4** are listed in Table 1, and a summary of important bond distances and angles is listed in Table 2 (for the full listing, see Table S4 in the Supporting Information). The molecular structure of **4** is illustrated in Figure 4 (H atoms omitted for clarity). There are two independent, but chemically identical, linear trinuclear complexes in the asymmetric unit (just one is shown in Figure 4). The trinuclear structure resembles that in **2** and **3**, with two ligands binding the three Dy^{III} ions in the same relative tridentate coordination pockets in each ligand. Five nitrate ions are bound in a chelating fashion, two to both Dy1 and Dy2 and one to Dy3. A coordinated DMF also binds to Dy3. Dy1 and Dy2 are 10-coordinate, and Dy3 is 9-coordinate. Dy–ligand distances fall in the range 2.292(2)–2.629(3) Å. The central Dy ions are bridged to the outer Dy ions through μ-O hydrazone bridges, with bridge angles in the range 116.55(9)–117.78(9)°. Dy–Dy distances fall in the range 4.085–4.100 Å.

The overall trinuclear structures of **2**–**4** are similar in the sense that the two ligands bind the three Ln^{III} ions in a spiral

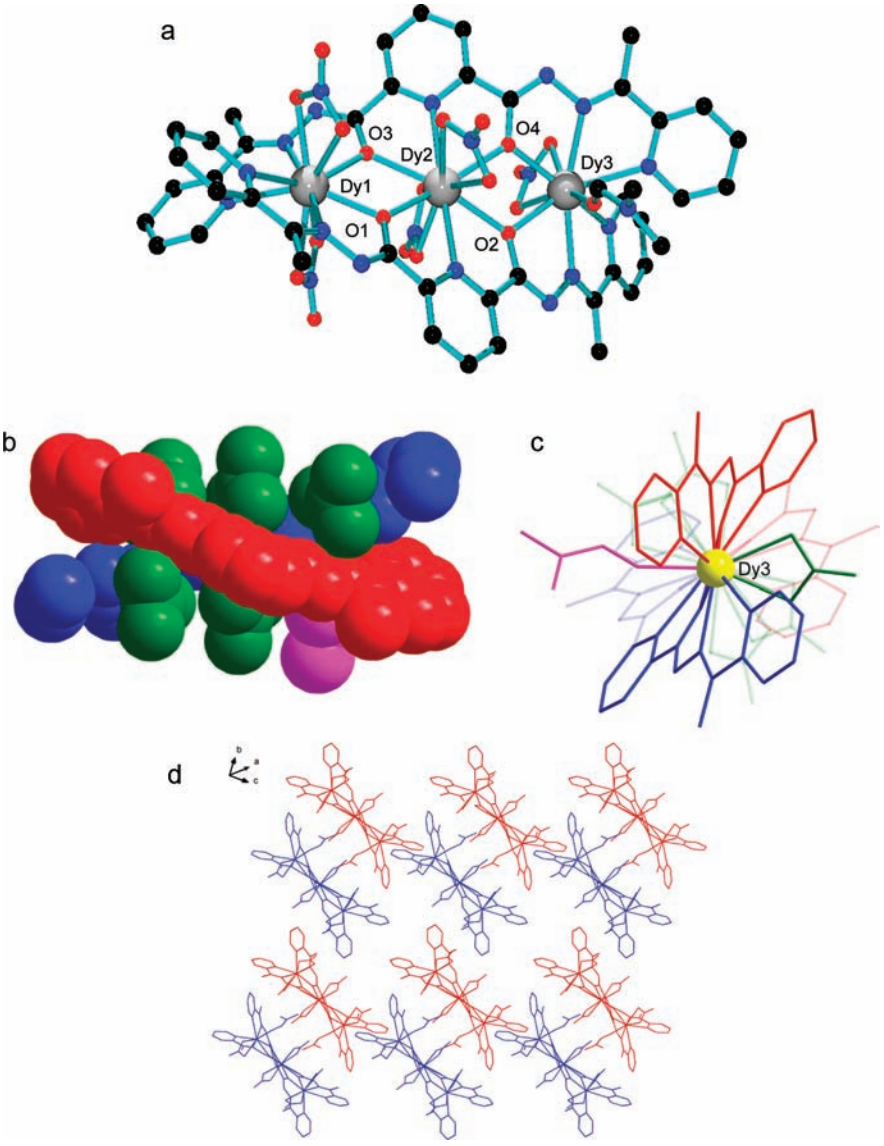

Figure 4. (a) Structural representation for complex **4**. (b–d) Structural representations for complex **4** emphasizing the helical arrangement.

dx.doi.org/10.1021/ic2022006 | *Inorg. Chem.* 2012, 51, 1028–1034

twisted fashion, yielding double-stranded helicate complexes. Parts a and b of Figure 4 illustrate this helical arrangement for **4**. The resulting chirality is induced by the coordination of achiral ligands to metal centers in the complex, leading to the formation of both homochiral enantiomers, ΔΔ and ΛΛ. The crystal packing diagram (Figure 4c) highlights the presence of both enantiomers for **4**, which are arranged in layers to allow for close packing. The ΔΔ isomer is indicated in red, while the ΛΛ isomer is in blue.

Structural Comparison between 2poap and 2pomp Complexes. In all reactions tried so far with 2poap, only mononuclear derivatives have been obtained, e.g., with Gd^{III}, whereas with 2pomp, there appears to be a preference for linear trinuclear complexes with La^{III}, Gd^{III}, and Dy^{III} examples. While this is not an exhaustive study, it does suggest some important differences that are ligand-based. The only significant difference between the ligands rests with the terminal pyridine moieties, whereas with 2pomp, the end piece would have more rotational flexibility because of the inability of the methyl group to participate in tautomerism and the likely increase in the donor strength of the adjacent hydrazone N atoms because of the presence of the methyl group as opposed to the NH_2 group in 2poap.

Magnetic Properties. The χT value for **1** at 300 K is 8.2 $cm^3 \cdot K \cdot mol^{-1}$, typical for a mononuclear Gd^{III} complex, and is essentially constant down to 2 K, as anticipated. Complex **2** is diamagnetic as would be expected. The magnetic data for complex **3** are shown in Figure 5, as χT vs temperature

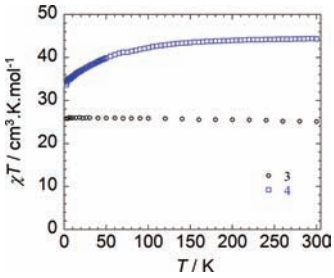

Figure 5. Variable-temperature magnetic data for **3** and **4** (see the text for fitted parameters for **3**).

obtained in a field of 0.1 T. The room temperature χT value (25.2 $cm^3 \cdot K \cdot mol^{-1}$) is consistent with the presence of three Gd^{III} ions (spin-only value 23.6 $cm^3 \cdot K \cdot mol^{-1}$). The χT values rise very slightly upon lowering of the temperature to 25.9 $cm^3 \cdot K \cdot mol^{-1}$ at 4 K, dropping a little below this temperature. Repeating the data collection at 0.01 T gave a slightly different plot with an almost constant χT value of ~24.5 $cm^3 \cdot K \cdot mol^{-1}$ down to 6 K, followed by a slight drop to 24.2 $cm^3 \cdot K \cdot mol^{-1}$ at 2 K. The difference in response as a function of field, and the slight rise in the moment upon lowering of the temperature at 0.1 T, could suggest the possible presence of weak intramolecular ferromagnetic exchange. Therefore, an attempt was made to fit the magnetic data to an isotropic exchange expression for a linear $S = {}^7/_2$ trinuclear model (eq 1, $S_1 = S_2 = {}^7/_2$) using *MAGMUN4.1*.[21] However, despite indications that J was positive and small (<0.2 cm^{-1}), the fitting could not be achieved without the use of a negative Weiss temperature correction (θ), which was significantly larger than J itself. Consequently, the fitting is not reported.

$$H_{ex} = -J\{S_1 \cdot S_2 + S_2 \cdot S_3\} \quad (1)$$

Ferromagnetic behavior has, however, been observed in a related Gd^{III}_2 complex bridged through μ-O linkages.[22]

Variable-temperature magnetic data for **4** are shown in Figure 5 as a plot of χT per mole as a function of the temperature. The χT value drops from 42.0 $cm^3 \cdot K \cdot mol^{-1}$ at 300 K to 28.4 $cm^3 \cdot K \cdot mol^{-1}$ at 2 K. The room temperature value is close to the theoretical value for three uncoupled Dy^{III} ions (theoretical value 42.5 $cm^3 \cdot K \cdot mol^{-1}$ for three noninteracting Dy^{III} ions; $S = {}^5/_2$, $L = 5$, $^6H_{15/2}$, $g = {}^4/_3$). While the decrease in χT upon lowering of the temperature could be attributed to antiferromagnetic exchange between the Dy^{III} ions, the drop to 2 K is more likely due to the depopulation of thermally accessible free ion states split by the ligand-field environment or the presence of a large anisotropy effect associated with the Dy^{III} ions. Magnetization data were obtained at varying field and temperature, as shown in Figure 6a. The nonsuperposition of the M vs H/T plots (Figure 6b) indicates the presence of significant magnetic anisotropy and/or thermally accessible low-lying excited states. Moreover, the magnetization value at 2.5 K and 7 T reaches 20.2 μ_B, somewhat lower than the anticipated value of 30.0 μ_B for three Dy^{III} ions, suggesting significant anisotropy in the system.

The combined effect of three bridged anisotropic Dy^{III} ions in **4** could lead to single-ion-based molecular magnetic relaxation and even SMM behavior. In order to elucidate possible SMM behavior, alternating-current (ac) magnetic measurements were performed in the frequency range 10–1500 Hz from 2 to 10 K under zero external field (Figure S1 in the Supporting Information). Below 10 K, a frequency-dependent ac signal was observed, indicating the presence of slow relaxation of the magnetization characteristic of SMMs. However, no full peaks were observed, which is mainly due to quantum tunneling of the magnetisation (QTM) often

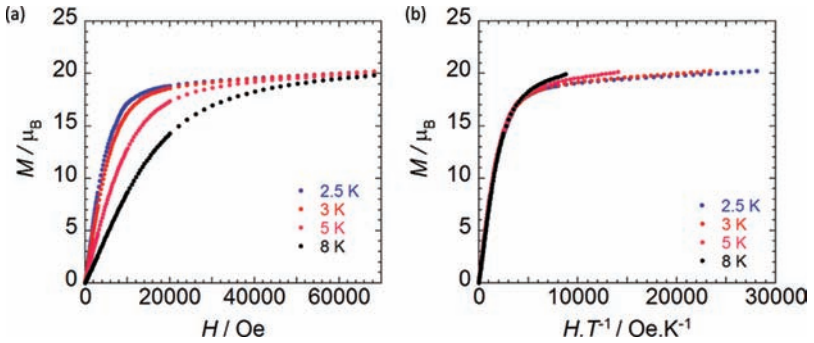

Figure 6. Magnetization (μ_B) vs (a) H and (b) H/T in the 2.5–8.0 K temperature range for **4**.

dx.doi.org/10.1021/ic2022006 | *Inorg. Chem.* 2012, 51, 1028–1034

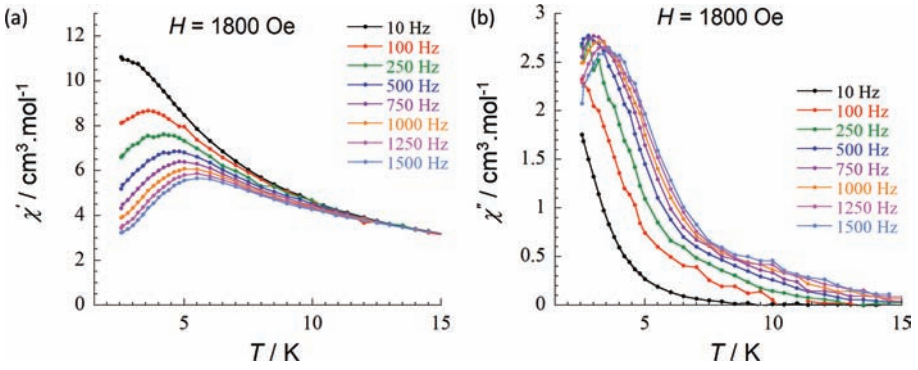

Figure 7. (a) χ' vs T and (b) χ'' vs T in the frequency range 10−1500 Hz with a bias dc field of 1800 Oe for **4**.

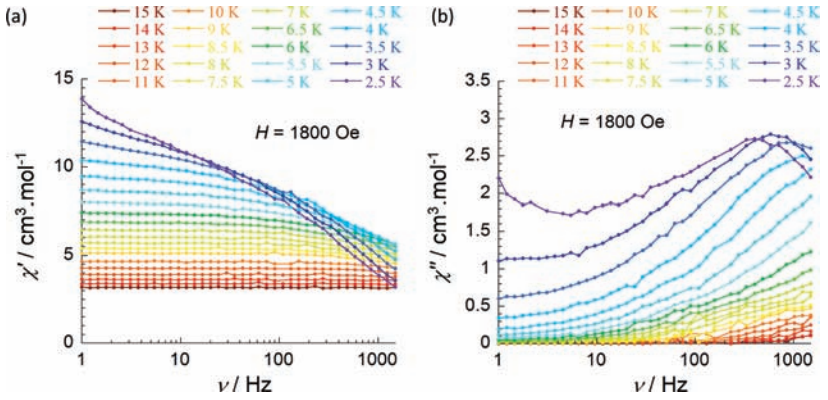

Figure 8. (a) χ' and (b) χ'' vs frequency temperature range 2.5−15.0 K with a bias dc field of 1800 Oe for **4**.

occurring in lanthanide SMMs.[22,23] In order to shortcut the QTM, a static direct-current (dc) field can be applied. Therefore, the data were remeasured in the presence of an optimum dc field of 1800 Oe to minimize the quantum tunneling, thus revealing a possible thermal relaxation regime. Under this field, peak maxima were observed below 5 K in the out-of-phase (χ'') vs T plot (Figure 7b), confirming SMM-like behavior. Such behavior under an applied field is often referred to as field-induced SMM behavior.[24,25] Plots of χ' and χ'' as a function of the frequency are shown in parts a and b of Figure 8, respectively, confirming the aforementioned field-induced SMM behavior. The observed thermally activated relaxation follows an Arrhenius-like behavior [$\tau = \tau_0 \exp(U_{eff}/kT)$], where the anisotropic energy barrier is calculated to be U_{eff} = 14 K, with a preexponential factor of $\tau_0 = 2.28 \times 10^{-6}$ s (Figure 9).

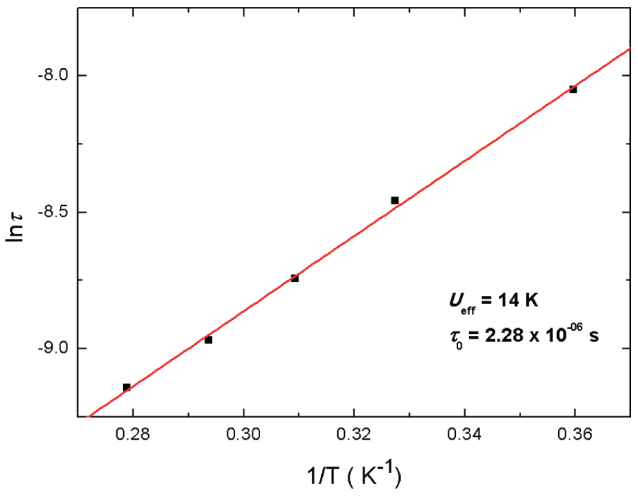

Figure 9. Magnetization relaxation time (τ) vs T^{-1} for **4** at an optimum field of 1800 Oe.

SUMMARY AND CONCLUSIONS

The increasing attention being focused on lanthanide complexes as potential SMM systems stems from fundamental single-ion properties, including the ground-state spin−orbit situation and the inherent anisotropic behavior typical of many lanthanide ions. Spin exchange per se has not been a primary objective, but assembling anisotropic lanthanide ion subunits in close proximity, in ordered arrangements, has been a targeted approach. *O*-Vanillin-based ligands, including those involving hydrazone functions, have formed a major focus in this area, producing examples of dinuclear and trinuclear Dy^{III} complexes exhibiting SMM behavior.[26−29] Simple vanillin and phenolic ligands have also produced linear and triangular trinuclear Dy^{III} complexes exhibiting slow magnetic relaxation.[30−34]

A characteristic structural feature of the polymetallic Dy^{III} complexes already reported (vide supra) is the combination of μ-O bridges from phenolic and hydrazone-based groups that connect the metal centers. In the case of **4**, the only bridging connections are the hydrazone O-donor atoms from the two heptadentate ligands. Linear trinuclear Dy^{III} complexes are not common,[33] and it is of interest to note that despite the larger ionic radius of the average Ln^{III} ion, compared with first-row transition-metal element ions, three Ln^{III} ions do fit well in the three tridentate pockets in 2pomp and maintain the arrangement of five-membered chelate rings typically observed in the characteristic [3 × 3] grids produced by this class of ligands. However, despite this, the higher coordination number

dx.doi.org/10.1021/ic2022006 | Inorg. Chem. 2012, 51, 1028−1034

expected for Ln^{III} ions seems to preclude square [$n \times n$] grid formation (vide infra).

The linear Dy^{III} complex **4** joins a select, but growing, group of polylanthanide complexes displaying slow magnetic relaxation at low temperatures and highlights the importance of the anisotropic properties of lanthanide ions as a whole in providing what are largely single-ion-based molecular properties. The importance of assembling groups of similar ions in close proximity rests with the notion that, by aligning the easy axes of these ions within the cluster appropriately, SMM character may result. This appears to be the case in **4**, but in-depth theoretical calculations will be required to examine this situation further. In this general context, square-grid-based arrangements of such ions might lead to a preferred group orientation of the easy axes, and possibly SMM behavior, rather than the perhaps more random orientations in typical 3D-type clusters. We are in the process of exploring routes to such systems, and preliminary results indicate that with an appropriately chosen ditopic ligand a square self-assembled [2 × 2] Dy^{III}_4 grid can be produced.[34] Studies are in progress to see whether this sort of architecture leads to slow magnetic relaxation.

■ ASSOCIATED CONTENT

Supporting Information

Figure S1 and Tables S1−S4. This material is available free of charge via the Internet at http://pubs.acs.org.

■ AUTHOR INFORMATION

Corresponding Author

*E-mail: lk.thompson@mun.ca.

■ REFERENCES

(1) Matthews, C. J.; Avery, K.; Xu, Z.; Thompson, L. K.; Zhao, L.; Miller, D. O.; Biradha, K.; Poirier, K.; Zaworotko, M. J.; Wilson, C.; Goeta, A. E.; Howard, J. A. K. *Inorg. Chem.* **1999**, *38*, 5266−5276.
(2) Thompson, L. K.; Matthews, C. J.; Zhao, L.; Xu, Z.; Miller, D. O.; Wilson, C.; Leech, M. A.; Howard, J. A. K.; Heath, S. L.; Whittaker, A. G.; Winpenny, R. E. P. *J. Solid State Chem.* **2001**, *159*, 308−320.
(3) Zhao, L.; Matthews, C. J.; Thompson, L. K.; Heath, S. L. *Chem. Commun.* **2000**, 265−266.
(4) Milway, V. A.; Niel, V.; Abedin, T. S. M.; Xu, Z.; Thompson, L. K.; Grove, H.; Miller, D. O.; Parsons, S. R. *Inorg. Chem.* **2004**, *43*, 1874−1884.
(5) Dawe, L. N.; Thompson, L. K. *Dalton Trans.* **2008**, 3610−3618.
(6) Dawe, L. N.; Abedin, T. S. M.; Thompson, L. K. *Dalton Trans.* **2008**, 1661−1675.
(7) Dawe, L. N.; Abedin, T. S. M.; Kelly, T. L.; Thompson, L. K.; Miller, D. O.; Zhao, L.; Wilson, C.; Leech, M. A.; Howard, J. A. K. *J. Mater. Chem.* **2006**, *16*, 2645−2659.
(8) Milway, V. A.; Abedin, S. M. T.; Niel, V.; Kelly, T. L.; Dawe, L. N.; Dey, S. K.; Thompson, D. W.; Miller, D. O.; Alam, S. M.; Müller, P.; Thompson, L. K. *Dalton Trans.* **2006**, 2835−2851.
(9) Dawe, L. N.; Shuvaev, K. V.; Thompson, L. K. *Inorg. Chem.* **2009**, *48*, 3323−3341.
(10) Thompson, L. K.; Zhao, L.; Xu, Z.; Miller, D. O.; Reiff, W. M. *Inorg. Chem.* **2003**, *42*, 128−139.
(11) Dawe, L. N.; Shuvaev, K. V.; Thompson, L. K. *Chem. Soc. Rev.* **2009**, *38*, 2334−2359.
(12) *SHELX97*: Sheldrick, G. M. *Acta Crystallogr.* **2008**, *A64*, 112−122.
(13) *DIRDIF99*: Beurskens, P. T.; Admiraal, G.; Beurskens, G.; Bosman, W. P.; de Gelder, R.; Israel, R.; Smits, J. M. M. *The DIRDIF-99 program system*; Technical Report of the Crystallography Laboratory; University of Nijmegen: Nijmegen, The Netherlands, 1999.
(14) Cromer, D. T.; Waber, J. T. *International Tables for X-ray Crystallography*; Kynoch Press: Birmingham, England, 1974; Vol. *IV*, Table 2.2A.
(15) Ibers, J. A.; Hamilton, W. C. *Acta Crystallogr.* **1964**, *17*, 781.
(16) Creagh, D. C.; McAuley, W. J. In *International Tables for Crystallography*; Wilson, A. J. C., Ed.; Kluwer Academic Publishers: Boston, 1992; Vol *C*, Table 4.2.6.8, pp 219−222.
(17) Creagh, D. C.; Hubbell, J. H. In *International Tables for Crystallography*; Wilson, A. J. C., Ed.; Kluwer Academic Publishers: Boston, 1992; Vol *C*, Table 4.2.4.3, pp 200−206.
(18) *CrystalStructure 3.7.0: Crystal Structure Analysis Package*; Rigaku and Rigaku/MSC: The Woodlands TX; 2000−2005.
(19) Watkin, D. J.; Prout, C. K.; Carruthers, J. R.; Betteridge, P. W. *CRYSTALS Issue 10*; Chemical Crystallography Laboratory: Oxford, U.K., 1996.
(20) Spek, A. L. *J. Appl. Crystallogr.* **2003**, *36*, 7−13.
(21) MAGMUN4.1/OW01.exe is available from the authors (http://www.ucs.mun.ca/~lthomp/magmun). It was developed by Dr. Zhiqiang Xu and OW01.exe by Dr. O. Waldmann. Source codes are not distributed. The origin of the programs should be quoted.
(22) Jeletic, M.; Lin, P.-H.; Le Roy, J. J.; Korobkov, I.; Gorelsky, S. I.; Murugesu, M. *J. Am. Chem. Soc.* **2011**, *133*, 19286−19289.
(23) Habib, F.; Lin, P.-H.; Long, J.; Korobkov, I.; Wernsdorfer, W.; Murugesu, M. *J. Am. Chem. Soc.* **2011**, *133*, 8830−8833.
(24) Lin, P.-H.; Smythe, N. C.; Gorelsky, S. I.; Maguire, S.; Henson, N. J.; Korobkov, I.; Scott, B. L.; Gordon, J. C.; Baker, R. T.; Murugesu, M. *J. Am. Chem. Soc.* **2011**, *133*, 15806−15809.
(25) Jurca, T.; Farghal, A.; Lin, P.-H.; Korobkov, I.; Murugesu, M.; Richeson, D. S. *J. Am. Chem. Soc.* **2011**, *133*, 15814−15817.
(26) Abbas, G.; Lan, Y.; Kostakis, G.; Anson, C. E.; Powell, A. K. *Inorg. Chim. Acta* **2008**, *361*, 3494−3499.
(27) Lin, P.-H.; Burchell, T. J.; Clérac, R.; Murugesu, M. *Angew. Chem., Int. Ed.* **2008**, *47*, 8848−8851.
(28) Guo, Y.-N.; Xu, G.-F.; Wernsdorfer, W.; Ungur, L.; Guo, Y.; Tang, J.; Zhang, H.-J.; Chibotaru, L. F.; Powell, A. K. *J. Am. Chem. Soc.* **2010**, *133*, 11948−11951.
(29) Guo, Y.-N.; Chen, X.-H.; Xue, S.; Tang, J. *Inorg. Chem.* **2011**, *50*, 9705−9713.
(30) Tian, H.; Guo, Y.-N.; Zhao, L.; Tang. J.; Liu, Z. *Inorg. Chem.* **2011**, *50*, 8688−8690.
(31) Tang, J.; Hewitt, I.; Madhu, N. T.; Chastanet, G.; Wernsdorfer, W.; Anson, C. E.; Benelli, C.; Sessoli, R.; Powell, A. K. *Angew. Chem., Int. Ed.* **2006**, *43*, 1729−1733.
(32) Hewitt, I. J.; Tang, J.; Madhu, N. T.; Anson, C. E.; Lan, Y.; Luzon, J.; Etienne, M.; Sessoli, R.; Powell, A. K. *Angew. Chem., Int. Ed.* **2010**, *49*, 6352−6356.
(33) Liu, C.-S.; Du, M.; Carolina Sañudo, E.; Echeverria, J.; Hu, M.; Zhang, Q.; Zhou, L.-M.; Fang, S.-M. *Dalton Trans.* **2011**, *40*, 9366−9369.
(34) Anwar, M. U.; Thompson, L. K.; Dawe, L. N.; Habib, F.; Murugesu. M. Unpublished results.